Anal Bioanal Chem (2009) 395:559–575
DOI 10.1007/s00216-009-3011-6

REVIEW

Exploring microdischarges for portable sensing applications

Y. B. Gianchandani · S. A. Wright · C. K. Eun · C. G. Wilson · B. Mitra

Received: 30 May 2009 / Revised: 20 July 2009 / Accepted: 23 July 2009 / Published online: 12 August 2009

Abstract This paper describes the use of microdischarges as transducing elements in sensors and detectors. Chemical and physical sensing of gases, chemical sensing of liquids, and radiation detection are described. These applications are explored from the perspective of their use in portable microsystems, with emphasis on compactness, power consumption, the ability to operate at or near atmospheric pressure (to reduce pumping challenges), and the ability to operate in an air ambient (to reduce the need for reservoirs of carrier gases). Manufacturing methods and performance results are described for selected examples.

Keywords Plasma · Discharge · Chemical · Radiation · Pressure

Introduction

In the past decade, microplasmas, or more generally microdischarges, have been investigated for their fundamental properties, and have been explored for uses in sensing applications. The intent, in most cases, is to incorporate microdischarge-based devices into portable, battery-powered analytical systems. Such systems also offer the potential benefits of requiring smaller samples, requiring smaller reagent volumes, requiring low power, and being less expensive to manufacture. Microdischarges, in such systems, can be used directly as transducers that produce electrical signals, or as a means of fractionating, ionizing, and exciting species, which are then analyzed by another component.

One promising application area for microdischarge-based devices is chemical sensing. Recent years have witnessed an increasing interest in miniaturized and portable systems for gas sensing, with applications ranging from environmental monitoring to homeland security. The emission spectrum of a discharge arises from spontaneous emission due to relaxation of excited chemical species to their ground states. A single observation can provide information regarding the composition of the ambient gas mixture. With modifications, emission spectroscopy of microdischarges can be extended to liquid-phase ambients.

There are other promising application areas for microdischarges as well. Conventionally, gas discharges have been used in the detection of radiation, as in Geiger counters and proportional counters. Miniaturized versions of these detectors utilize microdischarges. Recent work has also explored microdischarge-based pressure sensors for high-temperature environments: the relatively high electron and ion temperatures in microdischarges are less affected by the ambient temperature than are the transducing materials of most other sensors.

Microdischarges are similar to conventional discharges at larger scales in many ways, but have some important distinctions. As the distance between electrodes is de-

Y. B. Gianchandani (✉) · S. A. Wright · C. K. Eun
Center for Wireless Integrated Microsystems,
University of Michigan,
EECS Building, 1301 Beal Ave,
Ann Arbor, MI 48109-2122, USA
e-mail: yogesh@umich.edu

C. G. Wilson
Institute for Micromanufacturing,
Louisiana Tech University,
911 Hergot Avenue,
Ruston, LA 71272, USA

B. Mitra
Department of Electrical Engineering and Computer Engineering,
Rutgers University, 94 Brett Road,
Piscataway, NJ 08854-8058, USA

creased, the pressure at which lower currents and stable discharges exist is increased, up to and exceeding atmospheric pressure. Additionally, the relatively large ratio of surface area to discharge volume can make wall interactions more prominent. In DC-powered microdischarges, with the ionization dominated by secondary electrons, the glow region is proximal to the cathode and may overlap the high-field region. Another consequence of miniaturization is that very high power densities can be achieved without requiring high power: whereas conventional plasmas may operate at 10–500 mW/cm^2, microdischarges can be operated at 1–10 W/cm^2. Electron temperatures can be also relatively high, reaching 5–6 eV in microdischarges with small percentages of very high energy beam electrons. The distinctions between conventional and microscale discharges are reviewed in [1].

This paper explores how microdischarges can be used as a transduction element in different domains. "Gas-phase sensing" describes gas-phase sensing of chemical species and pressure; a brief review of different types of microdischarges is also included. "Liquid-phase sensing" describes microdischarge-based transducers for liquid-phase applications. "Radiation detection" describes microdischarges in the context of radiation detection. (Microdischarges used for display, surface treatment, destruction of gas pollutants, propulsion, in situ etching and deposition, sterilization, dental applications, and microwelding are beyond the scope of this paper.) All microdischarge-based transducers that are reviewed have some features with submillimeter dimensions, and are typically microfabricated. To the extent possible, all applications are explored from the perspective of microsystems, with emphasis on compactness and power consumption; the ability to operate at or near atmospheric pressure (to reduce pumping challenges); and the ability to operate in an air ambient (to reduce the need for a reservoir of carrier fluid).

Gas-phase sensing

Microdischarge-based gas-phase sensing has been performed through optical emission spectroscopy (as noted previously), or by other means such as mass or ion-mobility spectrometry. In contrast with conventional gas sensors, which depend on the absorption of selected analytes, microdischarge-based transducers are typically amenable to rapid and concurrent sensing of multiple species, and are less sensitive to the fabrication process and operating temperatures [2, 3].

A variety of DC- and RF-powered microdischarges have been explored in gas-phase microdischarge-based transducers, and have been reviewed in several papers [2–7]. RF-powered transducers utilize a dielectric layer between the electrodes and the plasma region, which prevents sputtering of the electrodes by bombarding positive ions to increase the electrode lifetime and minimize spectral interference. Additionally, RF-powered microdischarges do not heat the electrodes to the same extent as DC-powered microdischarges. DC-powered transducers require less external hardware for operation, such as a simpler power source. The lifetime of DC-powered transducers can be extended by utilizing pulsed discharge operation.

DC glow discharges in inert gases at atmospheric pressure have been used for optical emission spectroscopy, and have been attached at the ends of gas chromatographs (GCs) for decades [8]. GCs are one of the most powerful analytical instruments available today for the separation and identification of mixtures of gases. After separation, sensing or detection can be performed by a variety of means, ranging from mass spectrometry to simple thermal flow sensors. Recent efforts to miniaturize GCs [9, 10] present opportunities for integration with microdischarge-based transducers. An early paper describes a microplasma mass spectrometer coupled to a GC for halogen detection [11]. A review paper detailing the use of microdischarge-based transducers with GCs has also been published [12].

Several different varieties of microdischarges have been used to determine gas composition and pressure. These include the miniature inductively coupled plasma (ICP), microwave-induced plasma (MIP), capacitively coupled plasma (CCP), dielectric barrier discharge (DBD), micro-hollow cathode discharge (MHCD), planar DC microplasma, pulsed microarc, three-electrode microdischarge, arc-glow hybrid microdischarge, and multicathode pulsed DC microdischarge. A brief explanation of each follows.

Inductively coupled plasmas

ICPs are used in laboratory-scale devices for atomic emission spectroscopy. They require large volumes, large amounts of argon, water cooling, and have high power requirements of 1–2 kW. They typically generate plasmas at atmospheric pressure within a quartz tube with a helical coil wound around the tube providing energy at frequencies of 10–60 MHz. To allow for portable sensing in the field, several research groups have developed miniature ICP generators and have attached them to both Fabry-Perot interferometers and atomic emission spectrometers. ICPs differ from CCPs. The electric field in CCPs is parallel to the electrodes and accelerates ions from the plasma into the chamber walls, which heat and sputter the chamber. The electric field in ICPs is perpendicular to the electrodes, and thus does not accelerate the ions into the chamber walls and allows more power for ionization and excitation.

Miniaturized ICP (mICP) devices were developed by Hopwood's group [13]. The devices were microfabricated with planar load coils, with coil diameters of 5, 10, and

15 mm, to provide the inductive field. The devices operated at pressures between 0.1 and 10 Torr, and the optimum frequency for plasma generation was found to be 460 MHz. The electron temperature in the mICPs was found to be between 3 and 9 eV. These devices were modified to operate at 450 MHz in both argon and air [14]. They required 1.5 W for initiation, although they could be sustained with 350 mW. The mICPs were later operated in argon with increased plasma power and a silicon photodiode emission detector [15]. The limit of detection for SO_2 was 190 ppb using the 469.5 nm sulfur emission line with 3.5 W of input power. The most intense emissions existed adjacent to the planar coil beyond the plasma sheath, and this region was specifically observed to obtain the detection limit. The detection limit was later improved to 45 ppb in an argon environment and a model was developed to calculate the argon density, electron temperature, and SO_2 excitation rate [16]. However, the transducer still required a reduced-pressure environment.

Microwave-induced plasmas

Microwave-induced plasmas operating with frequencies in the gigahertz range have been used in optical emission spectrometry for decades and have recently undergone miniaturization. These plasmas exhibit lower gas temperatures than ICPs as the energy delivered to gas atoms and ions is lower than the energy delivered to electrons at these high frequencies.

Broekaert's group [17] reported microwave-induced microplasmas created in a dielectric channel with an external electrode at atmospheric pressure. Two quartz plates, 1 mm× 30 mm×90 mm, were bonded together creating a channel between them with dimensions of 0.9 mm×1 mm×90 mm. The microstrip electrode consisted of a small strip over the gas channel and was electroplated onto the structure. A 2.45-GHz microwave signal was applied with an input power of 10–40 W. Atomic emission spectroscopy was used with a monochromator to detect gaseous species and the 253.7 nm mercury emission line was used to obtain a detection limit of 0.05 μg/l [18]. A modified structure used sapphire substrates 30 mm in length and a helium ambient with an input power of 5–30 W. The transducer was used to break down halogenated hydrocarbons and detected $HCCl_3$ through the 912.1 nm chlorine emission line [19]. The configuration was further modified in a smaller device creating a microplasma jet, which extended 2 mm from the channel for enhanced detection [20]. With use of 30 W and an argon ambient, a detection limit of 0.01 μg/l was obtained using the 253.7 nm mercury emission line. However, an air cooler was used with this device. The channel was later reduced to have a 600 μm in diameter, and sulfur was detected at 0.1 μg/l [21]. These devices utilized external sources for microplasma ignition.

A coaxial structure was used to create a microwave microplasma jet, which extended 4 mm from the end of the coaxial line at atmospheric pressure [22]. The microplasma was created with a 2.45 GHz source and could be maintained with 2 W of power, after it had been initiated with around 10 W. The device operated in both argon and helium for over 30 h. It was used as a microdischarge-based transducer and the 912.1 nm chlorine emission line was used to detect $HCCl_3$, producing a detection limit of 66 ppb.

Iza and Hopwood [23] developed a microwave split-ring resonator plasma source for spectroscopic applications that operated at pressures from 50 mTorr to atmospheric pressure in argon and air. The initial resonator had a gap in which the microplasma was formed of 500 μm, a resonant frequency of 900 MHz, and a quality factor Q= 355. A modified resonator had a gap of 25 μm, a resonant frequency of 895 MHz, and obtained a quality factor Q= 142 [24–26]. At the resonant frequency, a voltage drop of 390 V was created across the 25-μm gap. This was high enough to initiate a microplasma at atmospheric pressure, indicating a self-igniting microplasma. The resonators consumed 3 W of power at atmospheric pressure, and operated at this pressure continuously for 50 h without significant electrode erosion. Carbon deposition was the noticeable result. The device achieved a detection limit of 200 ppb for SO_2 in argon at a reduced pressure of 2.5 Torr [25].

Capacitively coupled microplasmas

Capacitively coupled microplasmas have two dielectric layers in contact with the plasma and typically utilize the traditional 13.56-MHz excitation frequency. They benefit from long lifetimes as the dielectric layers separate the plasma from the external electrodes, which typically have a simple geometry. Capacitively coupled microplasmas have been operated in helium at atmospheric pressure, which eliminates the need for vacuum components but still requires an external gas source.

A capacitively coupled transducer was developed for absorption and emission analysis by Liang and Blades [27] and was later miniaturized in a fused-silica chip for atmospheric pressure operation [28]. The chip created microplasmas in a channel, confined by two quartz substrates. This channel was formed in the bottom substrate, 200–500 μm deep and 10 mm long, and the top substrate served as a lid. A pair of electrodes was used, one on the outer surface of each quartz substrate, forming a capacitively coupled discharge in the channel between them. Helium was used as the carrier gas, and the discharge was sustained with the application of 5–25 W of power at 13.56 MHz. When gas flowed through the channel with sufficient velocity, a microplasma jet was formed and it was analyzed using emission spectroscopy. Spectral measurements indicated the presence of OH, NH, N_2, N_2^+, and

helium. Yoshiki and Horike [29] reported a similar device, with the addition of an on-chip matching network to maximize power transfer. This group later reported capacitively coupled microplasmas in ceramic tubes and in comb electrode configurations, as well as a capacitively coupled discharge variation that they described as "ICP-type" [30].

A so-called stabilized capacitively coupled 27 MHz microplasma was created in helium at atmospheric pressure by Gross et al. [31]. The device used a silica tube with a 0.75-mm outer diameter and a 0.53-mm inner diameter as the dielectric, which was surrounded by two annular electrodes. Liquid cooling was used to prevent overheating and melting. The microdischarge-based transducer and accompanying spectrometer was attached to a GC. Seventeen different compounds were analyzed by examining the H_2, O_2, N_2, argon, and CO_2 emission lines.

Dielectric barrier discharges

DBDs are similar to capacitively coupled microplasmas as they have at least one dielectric layer in contact with the discharge, as opposed to an electrode. However, they operate at much lower frequencies, from a few hertz to several megahertz, usually in the kilohertz range. Typically, the power is applied by a square, sinusoidal, or pulsed high-voltage waveform. DBDs are highly transient, low-temperature, nonequilibrium discharges, formed from electrons of high mean energy and exist over a broad range of pressures [32, 33]. DBDs differ from other microscale high-frequency discharges in that they accumulate charge on the dielectric layer, known as memory voltage formation, which decreases the breakdown voltage of the gas. This effect is not seen at frequencies higher than those at which DBDs operate. Additionally, DBDs do not sputter the discharge electrodes, as the electrodes are covered by a dielectric layer. The discharges are traditionally created in helium and argon environments, and are employed in flat-panel plasma displays, in the treatment of surfaces, as mercury-free radiation sources, in plasma chemistry, and in excimer lamps.

Two different configurations are used in DBDs. The "volume discharge" configuration consists of two parallel electrodes separated by the gas medium and a dielectric layer, and the discharge is created in the gas medium. In contrast, the "surface discharge" configuration has an electrode on one side of a dielectric layer and a metallic feature on the reverse side of the dielectric, and the discharge is created around this feature. Both variations can operate at atmospheric pressure and consist of arclike discharge pulses that are approximately 10 ns in duration.

Cylindrical DBDs (C-DBDs) are created in a variation of the DBD configuration. They are formed in cylindrical dielectric alumina or silica tubes with electrodes wrapped around the tubes. This essentially uses two dielectric layers between the electrodes and confines the discharges between the electrodes along the tube length. These discharges are used as UV and VUV emission sources in pure argon, argon-N_2, and argon-air mixtures at pressures up to 500 Torr [34].

Niemax's group [35–37] reported low-pressure DBDs in helium and argon and used them with diode laser atomic absorption spectrometry for the detection of halogens in noble gas mixtures. The discharges consumed 0.5–1 W of power at frequencies of 5–20 kHz, at pressures of 4–120 Torr. Collinear beams of light from semiconductor diode lasers were passed through the DBDs, and were measured individually with photodiodes. This DBD configuration was used with a GC to detect halogenated and sulfured hydrocarbons through the elements fluorine, chlorine, bromine, iodine, and sulfur [38]. However, the use of absorption spectrometry necessitated low operating pressures and an inert ambient, which is challenging to provide in the context of portable applications.

Another application of DBDs was atomizing hydride-forming elements for their detection using an atomic absorption spectrometer as demonstrated by Zhu et al. DBD-based devices were used to detect arsenic [39], selenium, antimony, and tin at atmospheric pressure with an argon carrier gas [40]. A sine-wave voltage of 3.5–4 kV was used at a frequency of 20.3 kHz. Selenium, antimony, and tin had detection limits of 0.6, 13, and 10.6 μg/l, respectively. A new DBD atomizer was designed for use in atomic fluorescence spectrometry and was placed between a hollow cathode lamp and a photomultiplier tube detector [41, 42]. The device had a cylindrical configuration consisting of two concentric quartz tubes. The discharge was created in the center tube and a shield gas was contained in the outer tube. The detection limits for arsenic, selenium, tin, and lead were 0.04, 0.08, 0.11, and 0.27 μg/l, respectively.

A C-DBD capable of functioning at atmospheric pressure was developed as a microdischarge-based device for vapor sensing by Guchardi and Hauser [43]. A fused-silica capillary was used as the dielectric layer and two cylindrical electrodes separated from each other by 12 mm along the length of the capillary were used to capacitively couple energy into the tube. An AC voltage was used at a frequency of 20 kHz and 20 kV for a total of 8 W of power. Helium and argon were used as carrier gases and optical emissions were recorded with an external spectrometer for detection. Atomic emissions were examined and metal mercury vapor was detected with a detection limit of 200 ppb. Additionally, CO_2, CH_4, and ethanol vapors were detected using the 385.2 nm emission line, attributed to carbon, and the detection limits were found to be 90, 30, and 33 ppb, respectively. The device was operated for over 1 month without renewing the capillary tubing. This C-DBD was later used with an optical emission detector and coupled to a GC to detect inorganic [44] and organic [45, 46] compounds.

Another C-DBD design was utilized as an ionization source for an ion-mobility spectrometer at atmospheric pressure by Michels et al. [47]. Although the structure of this device was similar to that of the last one (i.e., having a dielectric capillary surrounded by two ring electrodes), it differed in that a microplasma jet was created by flowing a helium buffer gas through the capillary. The electrodes were spaced 12 mm apart and the closer of the two was 2 mm from the microplasma jet end of the capillary tube. A voltage of 5.5 kV was applied at a frequency of 33 kHz. Coupling the microdischarge to an ion-mobility spectrometer resulted in a detection limit of 55 ppb of 2-heptanone, and a minimum detection limit of 5 ppb.

Microhollow cathode discharges

Microdischarges created in cylindrical hollow cathode geometries, such as the circular metal-insulator-metal sandwich structure, are referred to as microhollow cathode discharges (MHCDs) [48]. In these structures, the discharges are spatially confined within the perforation through the structure, typically 10–500 μm in diameter. The two metal layers serve as separate anode and cathode electrodes, and the insulating layer thickness defines the discharge gap spacing. They operate at low and atmospheric pressures and can be formed using DC and AC voltages. MHCDs have high ionization efficiency, and the mechanisms of ionization include pendulum motion of electrons in the cathode perforation, secondary electron emission from the cathode, and Penning ionization. Traditionally, the term "hollow cathode" refers to a mode of operation in which the sustaining voltage drops as the current increases (i.e., the hollow cathode mode), but MHCDs commonly operate as normal or abnormal glow discharges. As a result, MHCDs have also been referred to as microstructure electrode discharges [36] and microdischarges [49].

Schoenbach et al. [50, 51] originally used the spectra produced as excimer light sources, designed to emit light at certain frequencies. In addition to the use of these devices in chemical sensors and light sources, research on MHCDs was motivated by uses in applications including instantly activated reflectors and absorbers for electromagnetic radiation in industrial applications, surface treatments, thin-film depositions, remediation and detoxification of gaseous pollutions, and gas lasers [48, 51].

A microdischarge-based transducer was created using MHCDs by Miclea et al. [36], which used DC voltages and helium and argon ambients at atmospheric pressure to detect chlorine and fluorine. The device used more than 2 W of power. An external spectrometer was used to detect emissions. The device had 30-μm-thick platinum electrodes with Al_2O_3 as an insulator. The perforation through the sandwich structure had a diameter of 100 μm and the electrodes were spaced 200 μm apart. CCl_2F_2 and $CHClF_2$ were decomposed and detected with a detection limit of 20 ppb for chlorine and fluorine using the 912.1 nm chlorine emission line or the 739.9 nm fluorine emission line. The devices were able to operate for more than 1 week in helium using a ceramic insulator and electrodes made from materials with low sputtering rates such as platinum and tungsten. This device was later used to detect ferrocene using the 371.9 and 344.1 nm emission lines of iron, with a detection limit of 500 ppb [52]. This device, with slightly different dimensions, was used with a GC [7, 12]. MHCDs were investigated between 40 Torr and atmospheric pressure to determine the gas temperature and electron density using absorption and emission spectroscopy [52]. An atmospheric pressure helium MHCD jet was also developed as a miniature ion source for mass spectrometry by Miclea et al. [53].

A subsequent effort by Eden's group [54, 55] utilized MHCDs for display applications. Arrays of microplasmas were fabricated with apertures of 80 μm×380 μm using ceramic tape as the insulating layer between electrodes. Xenon was excited between 45 and 480 nm to produce blue emissions, indicating the potential for applications in chemical sensing.

Planar DC microplasmas

Planar DC microdischarges are created above thin-film electrodes, typically patterned on a dielectric layer or glass substrate. The planar microdischarges are similar to MHCDs, but differ in that they are not confined in a circular cavity. Rather, they expand between electrodes; the expansion depends on the applied voltage and pressure. This also allows for multiple path lengths that are simultaneously available between electrodes. This makes the discharge gap a variable and permits a low breakdown voltage to be sustained, even as the pressure changes from the value that favors the minimum electrode spacing as discussed in [56, 57]. However, the microdischarges have been confined in chambers and channels when necessary. These microdischarges are commonly created using DC biases at pressures as high as 1 atm. Devices utilizing planar microdischarges can be fabricated using traditional IC microfabrication techniques on two-dimensional chips, making them attractive from a fabrication standpoint.

One of the first reported microdischarge-based transducers was developed by Manz's group [58] and utilized planar DC microplasmas in helium contained within a chamber. An external spectrometer was used for detection. The planar electrodes were patterned from chromium and gold deposited on a flat glass chip. Chambers of various geometric dimensions and volumes, from 50 to 450 nl, were created by wet etching a cavity in one chip and bonding it to the second chip, which supported the

electrodes. Microplasmas were created between 50 and 150 Torr, with an ideal pressure of 130 Torr in the 50-nl chamber. The microplasmas required 6 kV for ignition. Approximately 50 mW of power was dissipated in the plasma, with additional power dissipated in the 90-MΩ ballast resistor. With use of this device, methane was detected with a detection limit of 600 ppm by observing the CH diatomic emission band with a head at 431.3 nm. Enhanced operation was reported in a subsequent effort [59], detecting 50 ppm of methane in a helium background. In a separate effort, the device was coupled to a GC [60].

A DC microdischarge-based transducer was modified from the planar topography when it was fabricated by inserting two coaxial tungsten wire electrodes (50-mm diameter, 2-mm separation) into an 8-cm length of 250 mm inner diameter fused-silica capillary. The tungsten wires were secured by sleeves of Teflon tubing fit tightly over the capillary and wires [61]. This wire electrode design was then utilized to create four pairs of tungsten wire electrodes with tips 2 mm apart on a micofabricated chip (25 mm× 15 mm). Gas flowed through an etched channel in which the microplasmas were generated. Chlorine was detected at a detection limit of 8×10^{-10}g/s using the 479.5 nm emission line. The minimum utilized power was 260 mW.

Manz's group [62] also reported two planar DC microplasmas on a single chip, the first serving as an injector to a GC and the second as part of a sensor utilizing optical emissions following the columns. Samples of $CHCl_3$ and CH_2Cl_2 were introduced with background helium into the first injector microplasma, which was sustained except during brief intervals. In this way, it continually ionized and fragmented the molecules in the original sample. The level of fragmentation was controlled by the plasma parameters, such as electron energy, ion energy, and current density. This control allowed modulation of the flux of gas in the stream. When the plasma was briefly interrupted, it introduced a "plug" of unmodified sample into the system. Plugs between 5 and 50 ml were sent though the system, modulating the sample introduced into the columns. After samples had been separated in the columns, they were ionized and excited by the second microplasma device, coupled to a spectrometer. The detection limits for $CHCl_3$ and CH_2Cl_2 were approximately 1 μg/l. Two versions of the microplasma-based devices were fabricated; one used planar electrodes on a chip and a second used wire electrodes in a capillary as previously discussed. The device lifetime was limited by surface and electrode contamination.

Pulsed microarcs

Much of the work in microdischarge-based transducers has focused on steady-state plasmas as discussed already. Pulsed powering of microdischarges is attractive for two reasons: (1) power savings and (2) the possible utility of transient spectra. Pulsed microarcs are particularly attractive because they are high-temperature discharges and have a very intense glow, with spectral emission from UV to infrared.

Pulsed microarcs were used in a microdischarge-based transducer, which operated at atmospheric pressure in air [63]. The microdischarges were created between two planar electroplated copper electrodes on a Pyrex substrate. The temporal evolution of the spectra was examined to reduce the effects of broadband background emissions, and resolve closely spaced emission lines. Figure 1a shows a typical baseline measurement obtained from microarcs in an air ambient. For this measurement, the optical sampling duration encompassed the entire duration of the glow. The spectrum comprised bands corresponding to emission from atmospheric gases, superimposed on a broadband background. The reason for the broadband emission is not well understood, but is most likely a combination of blackbody emission [64] and recombination spectra from long-lived metastable species of nitrogen. This unpredictable broadband emission made detection of emission lines from analytes difficult.

There are further complexities that can arise from a number of sources. The large number of closely spaced rotational lines may not be adequately resolved by a modest spectrometer that is available with a portable instrument, and may manifest themselves as a continuum-like emission. The high operating temperature and pressure of these microdischarges potentially cause the closely spaced lines to broaden and overlap further. Doppler broadening, which is a result of random thermal motion of the emitting species, can increase dramatically at the elevated temperatures. Collision broadening, which is a result of interruption of light emission due to collisions, is also elevated in the high plasma density and elevated pressures that are found in the core of the arc. The combined impact of these complexities reduces the relative magnitude of targeted emission lines despite strong emission intensity from the microdischarge as a whole.

The typical temporal evolution of the spectrum is shown in Fig. 1b. The spectral emission is sampled in 2.1-ms-long windows of time at various delays from the termination of the microdischarge. The dominant line spectra decay rapidly compared with the wider background. If the goal is to detect dominant peaks, then samples that are short in duration and are taken with no delay provide a high ratio of signal-to-background spectral peak intensity when compared with longer samples (10 ms).

The afterglow contributes more of the background and less of line spectra. To the extent that the continuous broadband emission is correlated in time, and is not random, its impact can be reduced by correlated double sampling, i.e., observing the difference between two spectra taken at different times in a single afterglow period. Time-resolved spectroscopy thus provides the tool for real-time

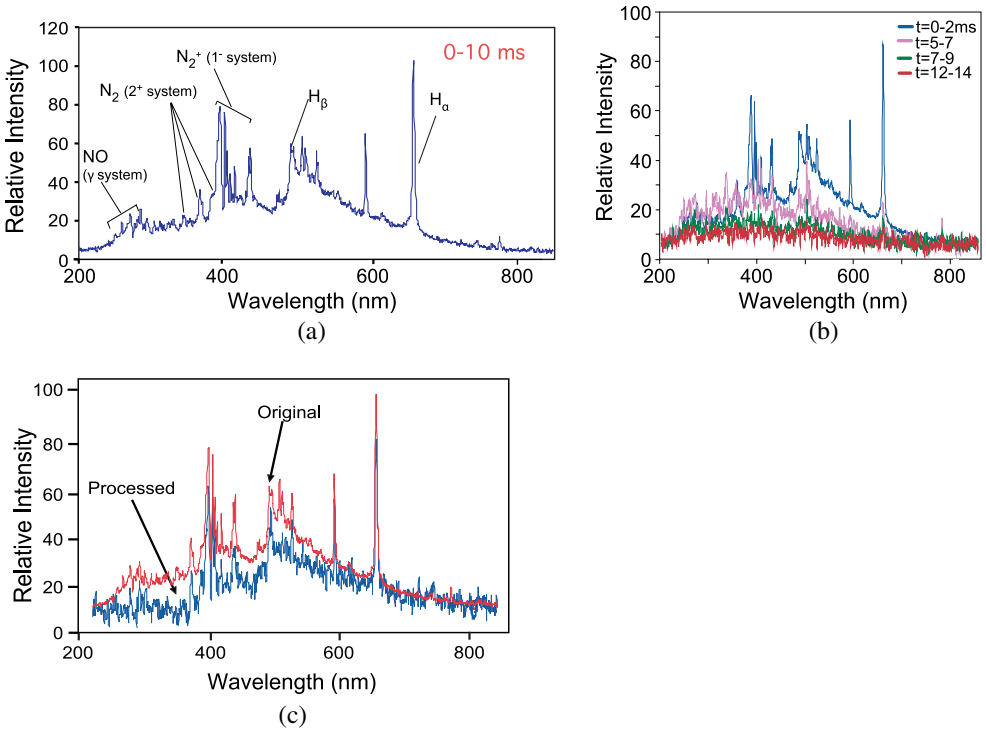

Fig. 1 **a** Spectrum of the microdischarge in air. **b** Time-resolved spectra of air. **c** When the continuous emission is subtracted from the spectrum at t=0, the resolution of the emission lines is enhanced

subtraction of the background to some extent. As shown in Fig. 1b, the afterglow spectra for t=7 ms and later were predominantly continuous emissions. To examine the benefits of correlated double sampling, the spectral emissions from t=7–9 ms and t=12–14 ms were subtracted from the t=0 spectrum. (It is important to note that the spectra were not scaled before subtraction as that would multiply the random noise.) Figure 1c shows the resulting spectrum, which had more discernible peaks, particularly in the 500–600-nm and 650–750-nm ranges. This permitted, for example, the identification of peaks for C_2 (Swan bands, 516.5 nm), which were otherwise less evident.

Three-electrode microdischarges

Additional power savings can be achieved by the use of multielectrode configurations. These schemes also offer a means of controlling discharge energy, and thereby tailoring the emission spectra.

A three-electrode (flashFET) microdischarge device was reported by Mitra and Gianchandani [63]. The flashFET (Fig. 2) utilized pulsed discharges and had two important structural differences from the previously described planar two-electrode DC structures: (1) it used a strategically located high-impedance electrode with a fixed bias and (2) one of the two low-impedance electrodes was capacitively powered to limit the discharge energy. In analogy with a field-effect transistor (FET), the high-impedance electrode was labeled the gate, the capacitively driven electrode was anodically biased and was labeled the drain, and the third electrode was cathodically biased and labeled the source. The drain was located next to the source, with a typical spacing of 200 µm, and the gate was further away, spaced 450 µm from the source.

To operate the device, the gate electrode was held at a high potential, but a large series impedance was used to ensure the current it supplied remained negligible. The drain electrode was allowed to charge up to the floating voltage potential, which was intermediate between the gate and source potentials. The energy stored in the drain-source

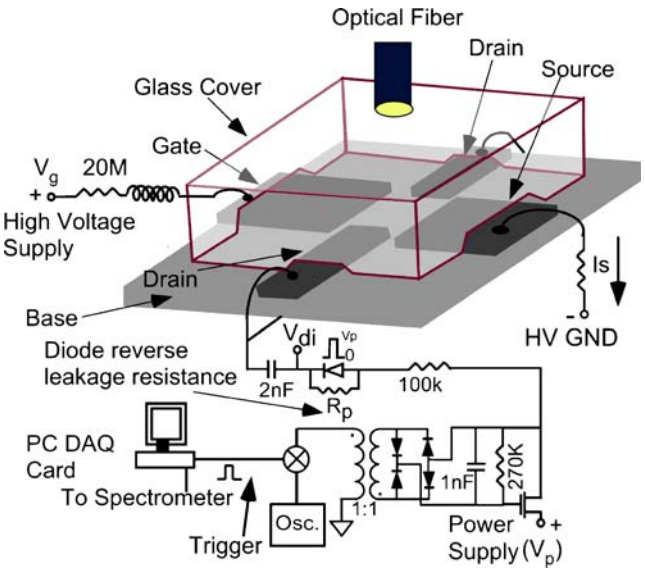

Fig. 2 The three-electrode flashFET, showing the electrode configuration, the glass cover, and the discharge circuit

capacitor was discharged by applying a small voltage pulse to the drain, which caused the potential to rise above the breakdown threshold. This approach consumed as much as 100 times less energy than a similar two-electrode microdischarge. This was due to its ability to deliver an extremely small amount of power to the discharge, a degree of control that was not possible with two-electrode devices. For example, a planar two-electrode device with a 200-μm discharge gap required 0.47 mJ over a duration of 6.5 ms, whereas a three-electrode device with a 200-μm drain-source spacing and a 450-μm gate-source spacing required 2.5 μJ over a duration of 200 μs, when operated at atmospheric pressure [63].

In preliminary tests, the monolithic three-electrode device was used to detect carbon in organic vapors using the 388.1 nm CN emission line. The line intensity was normalized to the nitrogen emission line (391.4 nm). Concentrations of 50 ppm were detected.

Arc-glow hybrid microdischarges

Further control of emission spectra can be achieved by using arc-glow hybrids, which are not conventionally employed in steady-state operation. The arclike discharges are driven by thermionic emissions, whereas the glowlike discharges are driven by secondary emission with a glow localized to the cathode surface (Fig. 3). In arc-glow hybrids, a localized cathode glow and a filamentary discharge originating from a cathode spot exist together [65]. The current waveform shows a steady component (corresponding to the glow discharge) with superimposed transient spikes that have arclike characteristics. The nature of the discharges is controlled by the circuit that powers the electrodes: a current-limiting resistor (typically between 1 kΩ and 1 MΩ) and a capacitor (which may be as small as a parasitic 2 pF) are used to provide the necessary hybrid behavior.

Arc-glow hybrids can provide a means of tailoring the spectral emissions from discharges. In Fig. 3, for example, it is evident that whereas long wavelengths dominate the spectral emission from the arclike discharges and short wavelengths are more prominent in glow discharges, the hybrids can have both properties. A handheld system reported in [65] utilized arc-glow hybrid microdischarges between two or three planar copper electrodes. The system included a holder for microchips on which the discharge electrodes were located; chips that were suitable for both gas-phase and liquid-phase samples could be accommodated. A custom circuit provided pulses of controlled delay and duration for the microdischarges and the synchronized data acquisition. A miniature spectrometer was used to capture the optical signals and to transfer the data to a wireless-enabled PDA. The system was powered by rechargeable 3.6-V Li-ion batteries, which made it portable. It was able to detect 17 ppm of acetone vapor in air at atmospheric pressure, without any preconcentration of vapors. The 388.6 nm CN emission line was used for detection and a response curve was measured for acetone vapor.

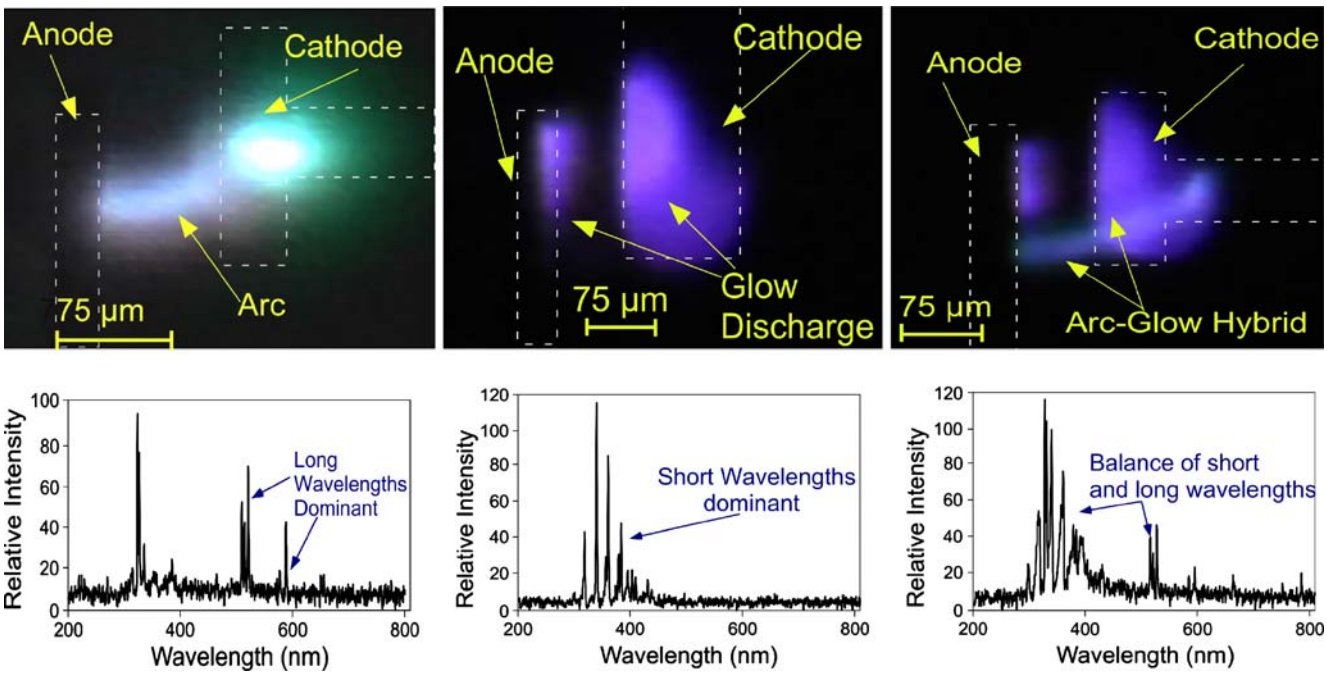

Fig. 3 Comparison of microdischarges: images and emission spectra of arclike discharges, glow discharges, and arc-glow hybrid discharges

Multicathode pulsed DC microdischarges and applications to pressure sensing

Microdischarge-based pressure sensors using pulsed DC microdischarges between multiple cathodes have been reported. They offer a direct electrical readout with a wide temperature range, and with greater scalability and robustness than conventional approaches. Devices utilizing pulsed microdischarges were well suited for high-temperature operation as the electrons had average thermal energies exceeding 2 eV (23,200 K) [66] away from the cathode, and higher energies proximal to it. This allowed the microdischarges to remain relatively unaffected by the ambient temperatures; the devices may operate above 1,000 °C and potentially down to cryogenic temperatures.

Pressure sensors suitable for high-temperature operation have uses in numerous industrial segments, including gas turbine engines, coal boilers, furnaces, and oil/gas exploration. A variety of microscale pressure sensing solutions have been explored, including Fabry-Perot and other optical techniques [67–69]. Diaphragm-type piezoresistive pressure sensors made from silicon carbide [70], sapphire [71], and even silicon [72] are capable of operating at temperatures as high as 800 °C.

The microdischarge-based pressure sensors measured the change in spatial current distribution with pressure [73]. As gas pressure increased, the mean free path of ionized molecules was reduced, and this changed the fractional current, $(I_1 - I_2)/(I_1+I_2)$, between two cathodes that were at different distances from the anode. At low pressures, the current favored the farthest cathodes, whereas at high pressures the opposite occurred. These sensors were different from ion gauges, which were not effective at atmospheric pressure because the small mean free path of the ions, 20–65 nm, made thermionic emissions difficult to detect [74].

The sensor structure consisted of several metal foil electrodes stacked within a cavity that served as a microdischarge chamber in a quartz chip (Fig. 4). A single disk-shaped anode served as the bottom of the chamber, the center electrodes were torus-shaped, and the top cathode was disk-shaped. To accommodate the wide range of operating temperatures, an arrangement that accommodated the expansion mismatch between the electrodes and substrate was necessary. The electrodes were lithographically patterned and etched from stainless steel foil, used for its robustness and oxidation resistance at high temperatures, by photochemical machining or spray etching [75]. Trenches of specified depths and a through-hole in the center were cut into the planar quartz substrate. Both mechanical and wet-etch processes could be used for this purpose. The electrodes were then assembled into the trenches, with the circular anode at the bottom and the ring-shaped cathode spaced above it. Ceramic epoxy held

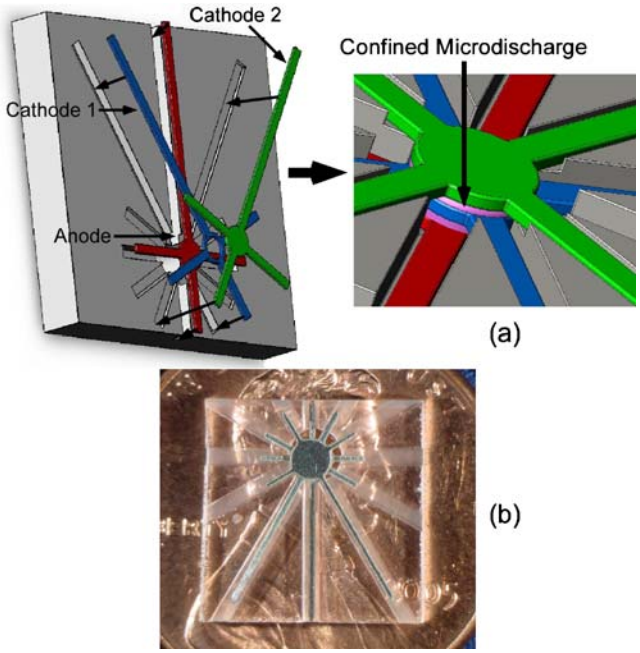

Fig. 4 **a** Sensor with electrodes above a quartz chip, illustrating placement, and the microdischarge chamber during operation. **b** Photograph of a sensor on a penny

the electrode leads and support arms in place, without adhering to the stainless steel. This allowed the leads and supports to expand separately from the quartz chip and the ceramic epoxy without buckling. A planar version of this device was also reported [73].

Figure 5 illustrates the differential current output from a typical sensor. The anode-cathode spacing in these sensors was set to produce measurable results up to 1,000 °C, for pressures between 10 and 2,000 Torr. Pulses were applied at a rate of 2–40 Hz to the sensors with voltages between 700 and 1,000 V, producing current pulses of 40–100-ns duration. The pulses consumed between 168 μJ and 6 mJ each.

The concept of determining pressure through discharge characteristics can also be expanded to different discharge-based devices, including spark plugs. Although these devices only have a single cathode, the characteristics of the discharges themselves and their pressure relationship can be utilized. Microdischarges were also used to control pressure in microsystem packages between thin-film titanium electrodes [76]. These effectively sputtered the electrode material, which bonded to nitrogen, oxygen, and other titanium-reactive gases within the package. By removal of the gases from the environment, the pressure inside the package was reduced by up to 168 Torr.

Liquid-phase sensing

Microdischarges have been applied to liquid-phase chemical sensing primarily in the context of testing water for

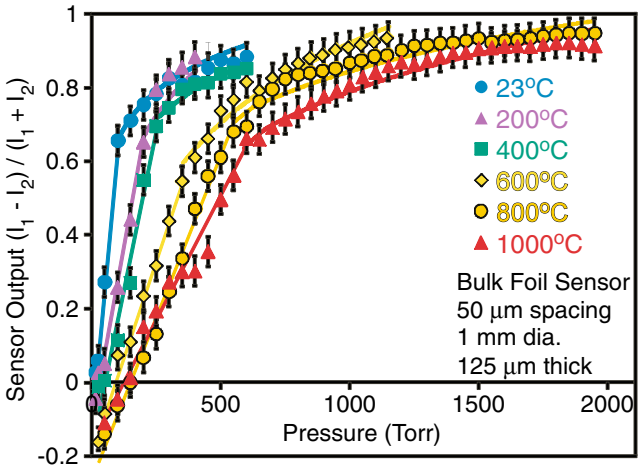

Fig. 5 Sensor output as a function of pressure with electrodes spaced 50 µm apart, 1 mm in diameter, and 125 µm thick. Each data point is the average of 100 measurements. Empirical curves for different temperature are indicated by *solid lines*

inorganic impurities. With the mounting challenges of supplying potable water to the growing population of the world, low-cost and portable microsystems can be envisioned for point-of-use analysis.

The conventional way to measure inorganic impurities in water was with an ICP spectroscopy system, which was relatively large and expensive. Although there were efforts to miniaturize ICP spectroscopy systems, these have not yet been applied to liquid-phase sensing. Electronic options include FET devices with ion-sensitive gate materials to analyze certain ionic species such as in [77]; these are not discussed in this review. Devices that ionized the sample and measured either the spectra or the mass transport characteristics promised the highest sensitivity and selectivity; several efforts were made to miniaturize these. A micromachined four pole electrostatic lens mass spectrometer and an RF ion-mobility spectrometer were developed [78, 79]. A few research groups developed systems that utilized microdischarge spectroscopy to analyze water impurities, and one review of this work is by Karanassios [2]. Several other plasma-based efforts are reviewed in the following section.

Spectroscopic microdevices for water chemistry analysis

A device reported by Jenkins and Manz [80] utilized a planar glass chip for sample containment with an attached peristaltic pump for water sample analysis. A wire-based platinum anode, which reduced wear and allowed anode repositioning, potentially allowed for long discharge time cycles. The device utilized 1–5 W of power. It was operated in an argon ambient, which reduced the background signals resulting from nitrogen and molecular oxygen constituents in air. Copper was detected in a 0.1 M $CuSO_4$ solution, but stability concerns were cited.

A similar strategy was followed in a device made by Cserfalvi and Mezei [81], creating an electrolyte cathode glow discharge (ELCAD). The ELCAD used a capillary tube with an electrolyte conductor at the cathode, and a pointed stainless steel rod as the anode. This allowed physical control of the anode–cathode spacing. The device also allowed for control of the flow rate of the liquid under test, which extended lifetimes and increased discharge stability. The device used 82 W of power at atmospheric pressure in air. Concentration detection limits of 14–34 ppb were realized for cadmium, zinc, copper, lead, and nickel.

Another glow discharge device was reported which used liquid as the cathode with an open air discharge [82]. This larger-scale device enabled detection of a wide variety of contaminants, including copper, iron, manganese, nickel, and lead in the 10–30 µg/l range, making the system a potentially viable component for drinking water monitoring.

Atmospheric pressure microplasma devices (MPDs) were reported by Karanassios' group [83, 84]. These devices were capable of analyzing liquid and powdered solid analytes. A new method of detection was used by introducing a coupled electrothermal, mini in-torch vaporization (mini-ITV) "dry" sample-introduction system to the low-power planar microplasma devices. AC-powered microdischarges were ignited on the patterned MPDs, which appreciably extended the electrode lifetimes, and the delivered liquid solutions were effectively dried on-chip. The resultant ability to integrate the optical signal over extended discharge periods allowed detection of impurities in the low-picogram to nanogram range. This included 2 pg for potassium, and 25 ng for lead. Mini-ITV also enabled measurement of analyte emission from microsamples of powdered solids as slurries.

A liquid sampling-atmospheric pressure glow discharge (LS-APGD) transducer for optical emission spectroscopy was developed by Davis and Marcus [85]. This device again utilized a liquid solution as an electrode. The delivery of the impurities was performed by local heating and volatilization, so the liquid could be either the anode or the cathode [86]. The use of heating to deliver impurities required higher currents (approximately 80 mA) than in other systems. However, the atmospheric discharge, which operated at these higher powers, was found to be more stable than other discharges. Analysis of the *I–V* curves of the discharge showed operation in the abnormal plasma regime. This regime traditionally offered higher current stability and also ionization by plasma heating. Analytical response curves for mercury, magnesium, sodium, and lead were demonstrated to have good linearity, with preliminary limits of detection determined to be in the range 1.1–2.0 ppm for 5-µL sample volumes.

A liquid electrode spectral emission chip (LEd-SpEC) was developed that miniaturized a significant number of components [87]. The LEd-SpEC concept utilized a pulsed DC microarc in air, at atmospheric pressure (Fig. 6). The device utilized a wet cathode, from which the water and impurities were sputtered into the glow discharge region. The liquid sample was delivered from an on-chip reservoir to the discharge region along a polymer-covered channel that had an embedded thin-film metal lead to provide the biasing. (Alternatively, the cathode could have been a porous material that wicked the water sample from the reservoir [65].) The liquid sample required a cathodic bias for operation. The use of a liquid-covered cathode also eliminated the problem of electrode wear. An optical fiber mounted proximate to the discharge delivered the optical signal to a pager-sized spectrometer, connected to a data-acquisition computer. To enable multiple water samples to be tested simultaneously, it was possible to integrate the dispersion optics of the spectrometer directly on the microdischarge device, so that a simple digital image could be used to perform the analysis [88].

To compensate for potential variations in the power density of the microdischarges, it was appropriate to use a differential sensing approach. One option was to use the emission intensity ratio of the target impurity to that of a signature nitrogen emission line from the air ambient. Another option was to use an internal chemical reference that was added to the test sample [89].

The basic LEd-SpEC device was fabricated on a glass substrate using a four-mask process. The first photo mask defined an etch pattern in the glass wafer, which created the water reservoir and delivery channel. The second mask patterned the thin-film platinum electrodes. Platinum was chosen for its lack of reactivity. The third mask provided a photoresist mold for a 30-μm-thick layer of electroplated copper, which was used as a sacrificial layer to produce the microfluidic channels. A 9-μm-thick layer of polyimide was then deposited on the structure, followed by an aluminum/titanium sputtered layer, which was lithographically patterned to serve as a hard mask for the dry etch of the polyimide. A hydrophobic coating was applied around the perimeter of the exposed liquid electrode, to prevent inadvertent transport of water along the surface that might be caused by the electrode bias.

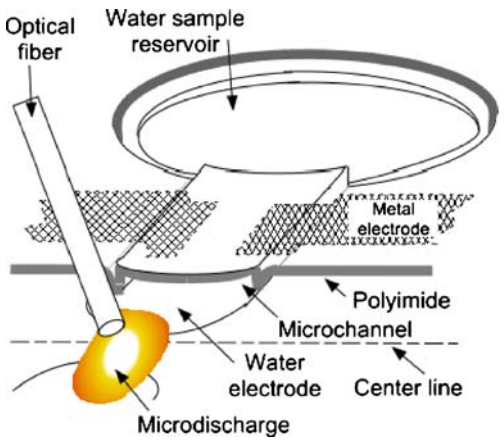

Fig. 6 The liquid electrode spectral emission chip. The test sample is cathodically biased and resides in a reservoir that leads to the microdischarge region through a channel. The anode can be a thin-film metal feature or another liquid sample; it does not affect the emission spectrum

LEd-SpEC devices and several variants detected lead, chromium, aluminum, and sodium. Figure 7 shows a spectrum obtained with a 5-ppm sample of lead in a solution containing nitric acid, which reduced the pH to 3.2. The characteristic emission lines at 280 and 405 nm were evident. Samples of chromium and aluminum at similar concentrations were also detected. Sodium had an extremely large spectral intensity at 589 nm, and was used for exploring the dynamic range of the device. The ratio of intensities for the sodium emission line to the 358 nm nitrogen emission line ranged from 0.24 for 10 ppm sodium, to 3.2 for 1,000 ppm sodium. This resulted in a log-linear response curve over several orders of magnitude, as the spectral intensity of the nitrogen emission line remained relatively constant. The LEd-SpEC device was also shown to be reusable: after sodium samples had been measured and the device had been cleaned with deionized water, no residual spectral signals were detected.

Moving forward, strategies need to be developed for further increasing sensitivity. As is typical with other microscale chemical sensors, some extent of preconcentration may be implemented for the sample. A lower-pH test sample, achieved by adding small quantities of nitric acid, may improve the detection limits. In preliminary tests it was observed that decreasing the pH of the test sample increased the intensity of the metal contaminants' emission lines relative to the nitrogen emission line. For example, for a 10-ppm-sodium sample, the ratio of sodium to nitrogen spectral intensities varied from 0.24 when the pH was 6, to 4.8 with a pH of 1.3. Similar increases of sensitivity were seen for 100-ppm-sodium samples. With the use of an appropriate preconcentration method, it can be expected that the detection limits of microdischarge-based transducers, such as LEd-SpEC, can easily be improved to 10–100-ppb levels.

Additional applications of microdischarges employing liquid electrodes

Since microdischarges at aqueous cathodes provide emission spectra that are characteristic of their dissolved inorganic impurities, the possibility of using the microdischarges as optical sources for fluorescent detection of biochemicals exists [90].

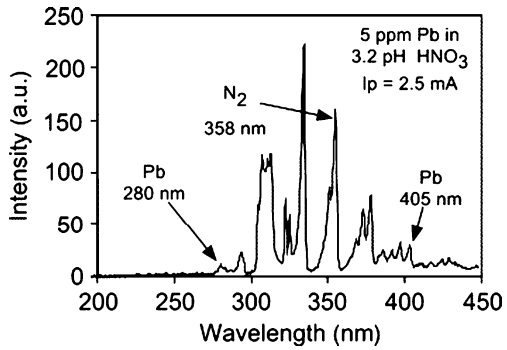

Fig. 7 Spectral emission from the liquid electrode spectral emission chip device while testing a water sample containing 5 ppm lead

A schematic of one possible configuration is shown in Fig. 8. The microdischarge was ignited across an air gap between a metal anode and a liquid reservoir containing a saturated salt solution, which served as the cathode. The ions in the cathode were sputtered into the glow region of the discharge and emitted a characteristic glow. Unwanted wavelengths were rejected by an optical filter that separated the microdischarge from the fluorescent sample. A dichroic color filter was chosen as the integrated bandpass filter owing to its low sensitivity to the light incident angle and its robustness. The sample was located in a reservoir or channel that could be part of a micro-total analysis system. The filtered emission from the discharge pulse followed optical path I (Fig. 8a), and stimulated fluorescence in the sample reservoir, which was detected along optical path II. These paths were orthogonal to minimize the signal feed-through from the microdischarge to the spectrometer.

The stacked device was fabricated by bonding the individual glass layers. A strip of metal foil was used as the anode for its superior wear-resistant properties. The discharge gap in this case was 400 μm. The biochemical reservoir was aligned with its center in line with the discharge gap to maximize the amount of light coupled from the discharge to the reservoir. This could be much smaller and could be a part of an overall microfluidic system. A photograph of the assembled device is shown in Fig. 8b.

For demonstration of the device as a fluorescence excitation source for biochemical sensing, calf thymus DNA samples labeled by SYBR green dye (Molecular Probes) were used. The liquid cathode was 20% w/v $BaCl_2$. The emission spectrum of barium provided 454 and 493 nm emission lines, corresponding to 25 and 97% excitation efficiency for this dye, respectively [91]. In the unfiltered spectrum, a number of emission lines characteristic to nitrogen and other atmospheric gases were also observed. The unwanted wavelengths were eliminated by the band-pass filter (350–500 nm). The two primary barium emission lines passed through the filter, excited the dye-labeled DNA, and induced fluorescence. This fluorescence (over 510–600 nm) was additionally filtered by a high-pass (more than 500 nm) optical filter, to reduce noise, before being imaged.

In a second series of experiments L-tryptophan was used as the sample. Unlike the SYBR dye tagged DNA, tryptophan had a very weak intrinsic fluorescence and required deep UV light for excitation and detection. A saturated $Pb(NO_3)_2$ solution was used to provide an emission (Fig. 9a) peak near 280 nm, which was characteristic of lead, and closely matched the excitation peak for tryptophan. The spectrum of the water sample was subtracted from that obtained with the tryptophan sample. Averaging over ±15 wavelengths using triangular weighted averaging reduced the random noise in the spectra. The characteristic broad peak of tryptophan fluorescence was detected between 300 and 450 nm (Fig. 9b).

Radiation detection

At the macroscale, gas-discharge-based detectors (e.g., Geiger counters) for detecting radiation are often favored for field use [92]. Known to be robust and relatively simple to use, these devices can operate over a large temperature

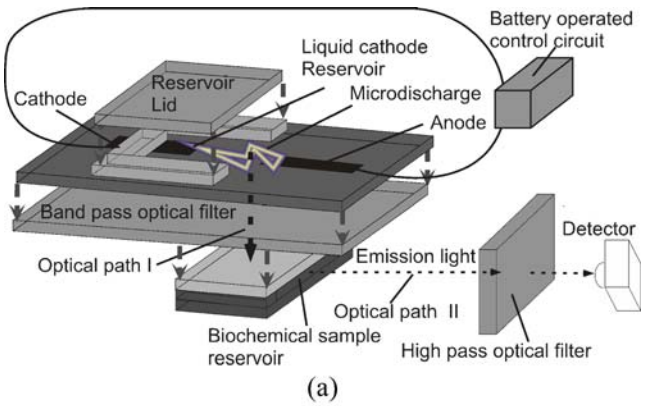

Fig. 8 **a** Exploded schematic of the optical source, the associated control circuit, and detector arrangement. *Short arrows* indicate the stacking order for the microchip, whereas *long arrows* indicate the two orthogonal optical paths, as noted. The chip is held vertically during operation. **b** Photograph of an assembled device

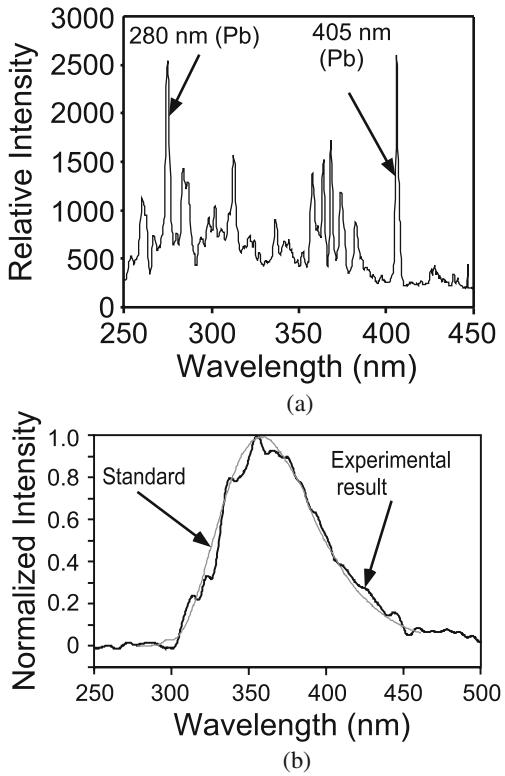

Fig. 9 **a** Filtered spectrum of the microdischarge source, with saturated (5g/10 ml) $Pb(NO_3)_2$ solution as the cathode, showing strong 280 nm lead emission lines. **b** Observed fluorescence emission spectrum from tryptophan

range and measure a wide range of radiation species and energies. Typically, gas-based radiation detectors utilize a gas volume that is under an applied electric field. Ionizing radiation (e.g., a beta particle) interacts with the gas atoms and creates charged particles. These particles are accelerated by the applied field, leading to electron multiplication (and depending on the degree of the field, in certain cases an avalanche breakdown) that produces a current pulse. One of the advantages of operating at higher applied electric fields (e.g., Geiger-Müller region) is the large inherent signal amplification via electron multiplication that occurs. This reduces the need for additional electronics such as amplifiers.

Gas-based detectors can be used to detect most radiation species. Beta particles interact directly with the gas atoms, which trigger current pulses. Gamma radiation is not detected directly by the gas atoms as the low density of the gas provides a low probability of interaction. Conventional Geiger counters detect gamma radiation by taking advantage of the photoelectric effect. Gamma rays, i.e., high-energy photons, bombard the metal encapsulation (e.g., a Geiger-Müller tube) of the sensing gas, producing photoelectrons within the tube that trigger avalanche current pulses. The use of metals to convert gamma rays into photoelectrons is well established [93–96]. Other gas-based detectors use high-pressure, high-Z (i.e., heavier gases such as Kr and Xe) fill-gases [97] to interact with the gamma rays.

For gas-based neutron detection, the ionization mechanism cannot be applied since neutrons have no electrical charge. However, gas-based detectors can be adapted for neutrons by incorporating nuclides with large neutron cross sections (e.g., ^{3}He, ^{10}B, and ^{235}U) in high-pressure (1–10-atm) environments [92, 98, 99]. These nuclides react with the neutrons to create charged particles (e.g., protons and alpha particles), which can trigger electron avalanches in the fill-gas. The major source of background noise is high-energy photons, which can register similar energies and are difficult to differentiate from the neutrons.

Gas-based radiation detectors with submillimeter feature sizes have been under investigation for some time. In the late 1960s, Charpak et al. [100] used gas avalanche detectors to achieve position localization of charged particles using an array of very thin, closely spaced wire electrodes. The multiwire proportional chamber was able to achieve submillimeter accuracies over detection areas exceeding a square meter, with fast recovery times and very high count rates.

Advancements in lithographic manufacturing technologies have played a key role in the development of microfabricated gas-based radiation detectors. Planar configurations have provided an increase in structural stability, as well as greater uniformity in detector performance. These configurations tended to operate in a lower-field region, at the cost of signal amplification, to avoid spurious discharges that could potentially damage the electrode structures. One of the first micropatterned detectors involved a microstrip electrode structure with alternating thin metal strips for the anode and cathode (typically, 10 and 100 μm, respectively) laid on an insulating support [101, 102]. Since then, several other detector structures have been developed, including the MICROMEGAS [103]. It used a small-gap (50–100-μm-wide), parallel-plate design where the radiation-induced electrons were pulled through a dense wire micromesh structure (cathode) located between the plates, leading to signal multiplication and finally collection at the anode strip. The micro-CAT [104] used a metal electrode plane (cathode) with a fine mesh grid of machined holes. Localized electron multiplication occurred through the hole structure and the electrons were accelerated toward an anode plane. It was coupled to a 2D resistive readout system. The gas electron multiplier (GEM) [105] was essentially a thin insulating foil (about 50-μm-thick Kapton foil) that was metallized on both sides and perforated with holes. Similar to the micro-CAT, the electrons were pulled through the holes by the electric field and were then cascaded either through another GEM structure for further multiplication or to a 2D resistive readout system. With a

focus on high spatial resolution, each device was targeted for position-sensing applications, such as medical imaging and nuclear particle tracking [105, 106], and was not necessarily targeted for environmental or security applications.

Presently, there is interest in designs intended for environmental monitoring and homeland security applications. In these contexts, wireless signaling is sometimes important. Individually, microfabricated detectors could be used in applications for which the weight or space is at a premium, e.g., micro air vehicles. As elements of a network, the detectors may facilitate reconfigurable deployment in public spaces (e.g., football stadiums, amusement parks, and shopping malls), or in dangerous and inaccessible environments (e.g., contaminated or remote areas) [107, 108].

Under appropriate conditions, the microdischarges can concomitantly produce a wireless signal. Gas-based discharges were employed for wireless communication in the mid-1890s using Marconi's spark gap transmitters [109]. The discharge gaps were relatively large (on the order of centimeters), achieving transmission distances on the order of kilometers. In 1901, Bose utilized these discharges within waveguides to generate microwaves. More activity on this topic has been reported [110].

A microfabricated beta-particle detector with inherent wireless signaling capability was recently described [111]. The device structure consisted of a square chamber with a central cathode and a peripheral anode (Fig. 10a). In contrast with most conventional Geiger counters, this chamber was at atmospheric pressure. The region proximal to the cathode had a weak electric field and was called the drift region, whereas that adjacent to the anode was the high-field region, where the avalanche occurred. The resulting microdischarge transmitted a wideband electromagnetic signal that was detected using commercial AM/FM receivers [112, 113].

This type of microdischarge-based detector was fabricated from a glass-silicon-glass stack, using a simple two-mask process. The first mask defined a boron diffusion pattern on the silicon wafer; boron doping served as an etch stop in a subsequent etch. The second mask was used on the backside of the silicon wafer, and defined the removal of a protective oxide layer to reveal the region that was wet-etched for the gas cavity. The side walls of the cavity were formed by the tapered <111> silicon crystal planes that surrounded the perimeter [114]. Glass wafers were bonded to the silicon wafer to form the top and bottom of the cavity, with the option to perforate the glass to facilitate lead transfer [115–117].

A microfabricated device with wireless signaling for gamma detection was reported [118]. Its structure consisted of a glass substrate with electroplated copper electrodes and assembled on top of it a micromachined conversion layer patterned from bulk metal (Fig. 10b). When gamma radiation interacted with the metal conversion layer (MCL), photoelectrons were emitted and ionized the surrounding gas, triggering avalanche current pulses and RF signaling. For lower gamma ray energies, the photoelectric effect dominates, and one photoelectron is generated per incident gamma ray. At higher gamma ray energies (above 1 MeV), Compton scattering dominates, which results in multiple photoelectrons being generated in the metal layer per gamma ray. Higher-density metals (e.g.,

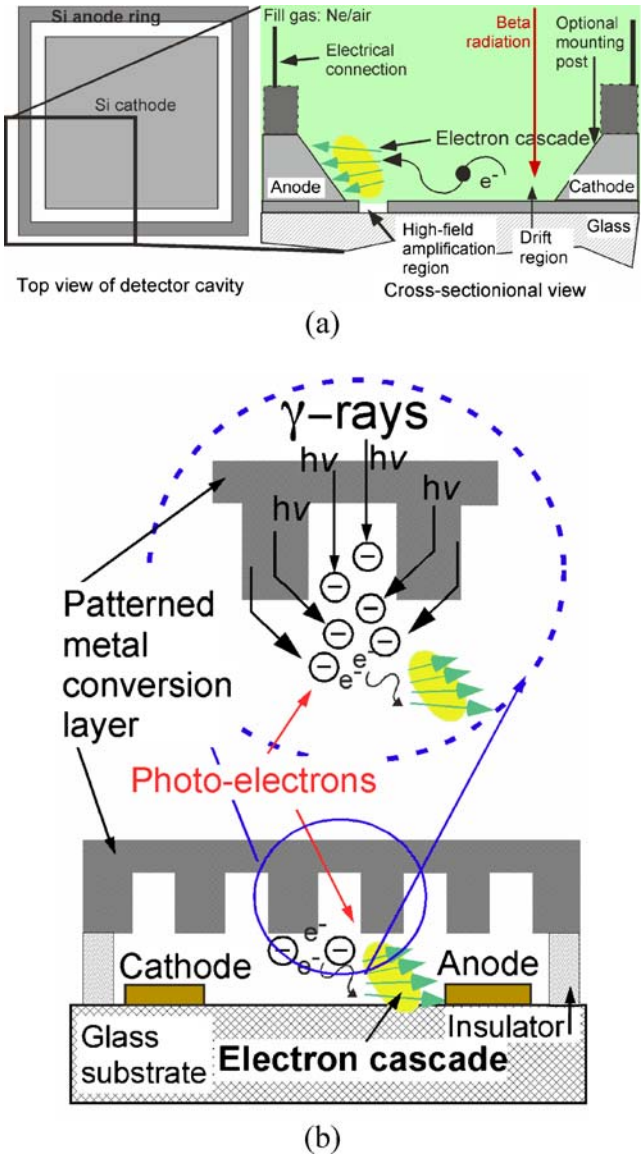

Fig. 10 **a** Microfabricated beta detector. The structure utilizes dissolved silicon bonded to glass as the anode-cathode configuration. Beta radiation passing through the drift region creates liberated electrons, which are accelerated in the amplification region and create an electron cascade. **b** Microfabricated gamma detector. Cross section of a gamma detector with a patterned bulk metal conversion layer. As gamma radiation interacts with the metal conversion layer, the generated photoelectrons ionize the surrounding gas between the electrodes, initiating a gas discharge and current pulse

platinum-rhodium) are desirable for the MCL because of their higher interaction probabilities. Also, photon interactions in the MCL increases with metal thickness, but the resulting photoelectrons have a higher probability of reabsorption back into the metal layer, instead of ejection. Hence, the photoelectron mean free range should be comparable to the MCL thickness. If the surface area exposed to the fill-gas is increased, the reabsorption probability of the photoelectrons decreases [94, 95]. Trenches and grooves etched into the MCL can help in this respect, and can be defined by microelectrodischarge machining [119]. This type of simple structure can be fabricated by bonding a glass substrate with planar thin-film metal electrodes to the MCL, separated by an insulating layer.

The fabricated devices were tested with weak radioisotope sources, using both wired and wireless measurements. Figure 11a illustrates the detection of beta particles from a 0.1 μCi source of ^{90}Sr using microdischarge-based detectors with

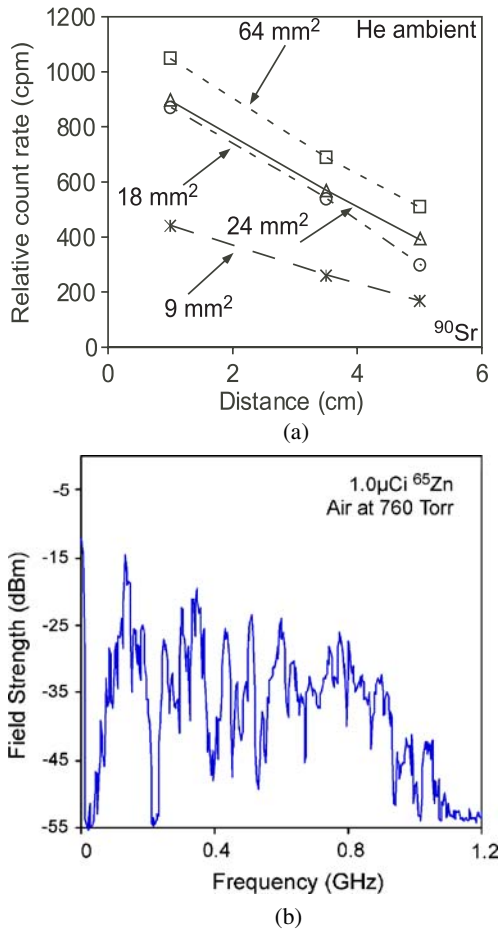

Fig. 11 **a** Detection of beta particles from a 0.1 μCi ^{90}Sr source using helium-filled microcavities of various volumes [111]. Count rates decrease with decreasing cavity sizes. **b** A wireless signal obtained from the detection of gamma radiation measured by an antenna placed 30 cm from the detector

various cavity dimensions (8×8, 4×6, 3×6, and 3×3 mm^2) as a function of source-to-detector spacing. The fill-gas was helium. As expected, count rates increased with larger detection areas and decreased with larger source-to-detector separation. Figure 11b shows wireless measurements of gamma radiation of 1.0 μCi from ^{65}Zn. The wireless signal displayed a bandwidth extending beyond 1.2 GHz.

The design of the microfabricated detectors permitted flexibility in sizing and integration with other types of detectors, so they could be used to form composite structures with greater functionality. For example, beta and gamma detectors could be integrated on the same chip, which may provide information as to the type of radioisotope emitter.

Conclusions

The preceding sections reviewed the use of microdischarge-based transducers. The utility of microdischarges and the diversity of potential applications are self-evident from the examples that were discussed. Compared with other transduction mechanisms, some of the general benefits of microdischarges include direct electrical or electro-optical transduction, as in the chemical sensors that use emission spectroscopy; the ability for wireless RF signaling, as in the radiation detectors; and the ability to operate under harsh environmental conditions, as in the pressure sensors. These examples also illustrate how the devices can be manufactured, exploiting lithographic manufacturing as appropriate, but much work remains in this area. The choice of materials, in particular, electrode materials, will affect not only the performance of the sensors but also device longevity. There are also a number of research challenges. The ability to control the ionization level, the energy, and the spatial and temporal extent of microdischarges is an important goal. A few pathways to possible solutions, such as multielectrode discharges and arc-glow hybrids, have been discussed in this paper. For most aspects of microdischarge behavior, the ability to perform predictive modeling is still quite limited. The availability of reliable models is essential to spur application of microdischarges. As these capabilities are improved, new devices and applications are certain to emerge.

Acknowledgements The authors are grateful to Long Que, Ranjit Gharpurey, Mike Zorn, Marc Anderson, Amy Wendt, Victor Kolobov, Robert Arslanbekov, Ravi Selvaganapathy, and others who have collaborated on various parts of the effort over the years. Portions of the work described here have been supported by the National Science Foundation, the Sea Grant Institute, and the Water Resources Institute. Y.B.G. acknowledges support through the IR/D program while working at the National Science Foundation. The findings do not necessarily reflect the views of the National Science Foundation.

References

1. Foest R, Schmidt M, Becker K (2006) Int J Mass Spectrom 248:87–102
2. Karanassios V (2004) Spectrochim Acta Part B 59:909–928
3. Miclea M, Franzke J (2007) Plasma Chem Plasma Process 27:205–224
4. Broekaert J (2002) Anal Bioanal Chem 374:182–187
5. Franzke J, Kunze K, Milcea M, Niemax K (2003) J Anal At Spectrom 18:802–807
6. Broekaert J, Siemens V (2004) Anal Bioanal Chem 380:185–189
7. Franzke J, Miclea M (2006) Appl Spectrosc 60:80a–90a
8. Braman R, Dynako A (1968) Anal Chem 40:95–106
9. Lambertus G, Elstro A, Sensenig K, Potkay J, Agah M, Scheuering S, Wise K, Dorman F, Sacks R (2004) Anal Chem 76:2629–2637
10. Agah M, Lambertus G, Sacks R, Wise K (2006) J Microelectromech Syst 15:1371–1378
11. Brede C, Lundanes E, Greibrokk T, Pedersen-Bjergaard S (1998) J High Resol Chromatogr 21:633–639
12. Miclea M, Okruss M, Kunze K, Ahlman N, Franzke J (2007) Anal Bioanal Chem 388:1565–1572
13. Yin Y, Messier J, Hopwood J (1999) IEEE Trans Plasma Sci 27:1516–1524
14. Hopwood J (2000) J Microelectromech Syst 9:309–313
15. Minayeva O, Hopwood J (2002) J Anal At Spectrom 17:1103–1107
16. Minayeva O, Hopwood J (2003) J Anal At Spectrom 18:856–863
17. Engel U, Bilgic A, Haase O, Voges E, Broekaert J (2000) Plasma Sources Sci Technol 9:1–4
18. Engel U, Bilgiç A, Haase O, Voges E, Broekaert J (2000) Anal Chem 72:193–197
19. Bilgiç A, Voges E, Engel U, Broekaert J (2000) J Anal At Spectrom 15:579–558
20. Schermer S, Bings N, Bilgic A, Stonies R, Voges E, Broekaert J (2003) Spectrochim Acta Part B 58:1585–1596
21. Broekaert J, Siemens V (2005) IEEE Trans Plasma Sci 32:560–561
22. Stonies R, Schermer S, Voges E, Broekaert J (2004) Plasma Sources Sci Technol 13:604–611
23. Iza F, Hopwood J (2003) IEEE Trans Plasma Sci 31:782–787
24. Iza F, Hopwood J (2004) IEEE Trans Plasma Sci 32:498–504
25. Hopwood J, Iza F (2004) J Anal At Spectrom 19:1145–1150
26. Hopwood J, Iza F, Coy S, Fenner B (2005) J Phys D 38:1698–1703
27. Liang D, Blades M (1988) Anal Chem 60:27–31
28. Bass A, Chevalier C, Blades M (2001) J Anal At Spectrom 16:919–921
29. Yoshiki H, Horike Y (2001) Jpn J Appl Phys 2 40:L350–L362
30. Taniguchi K, Fukusawa T, Yoshiki H, Horiike Y (2003) Jpn J Appl Phys 1 42:6584–6589
31. Gross R, Platzer B, Leitner E, Schalk A, Sinabell H, Zach H, Knapi G (1992) Spectrochim Acta Part B 47:95–106
32. Gibalov V, Pietsch G (2000) J Phys D 33:2618–2636
33. Becker K, Kogelschatz U, Schoenbach K, Barker R (2004) Non-equilibrium air plasmas at atmospheric pressure. Institute of Physics, Bristol
34. Masoud N, Martus K, Becker K (2005) J Phys D 38:1674–1673
35. Miclea M, Kunze K, Musa G, Franzke J, Niemax K (2001) Spectrochim Acta Part B 56:37–43
36. Miclea M, Kunze K, Franzke J, Niemax K (2002) Spectrochim Acta Part B 57:1585–1592
37. Kunze K, Miclea M, Musa G, Franzke J, Vadla C, Niemax K (2002) Spectrochim Acta Part B 57:137–146
38. Kunze K, Miclea M, Franzke J, Niemax K (2003) Spectrochim Acta Part B 58:1435–1443
39. Zhu Z, Zhang S, Lv Y, Zhang X (2006) Anal Chem 78:865–872
40. Zhu Z, Zhang S, Xue J, Zhang X (2006) Spectrochim Acta Part B 61:916–921
41. Zhu Z, Liu J, Zhang S, Na X, Zhang X (2008) Anal Chim Acta 607:136–141
42. Zhu Z, Liu J, Zhang S, Na X, Zhang X (2008) Spectrochim Acta Part B 63:431–436
43. Guchardi R, Hauser P (2003) J Anal At Spectrom 18:1056–1059
44. Guchardi R, Hauser P (2004) J Chromatogr A 1033:333–338
45. Guchardi R, Hauser P (2004) Analyst 129:347–351
46. Guchardi R, Hauser P (2004) J Anal At Spectrom 19:945–949
47. Michels A, Tombrink S, Vautz W, Miclea M, Franzke J (2007) Spectrochim Acta Part B 62:1208–1215
48. Stark R, Schoenbach K (1999) J Appl Phys 85:2075–2080
49. Frame J, Wheeler D, De Temple T, Eden J (1997) Appl Phys Lett 71:1165–1167
50. Schoenbach K, El-Habachi A, Moselhy M, Shi W, Stark R (2000) Phys Plasmas 7:2186–2191
51. Moselhy M, Petzenhauser I, Frank K, Schoenbach K (2003) J Phys D 36:2922–2927
52. Miclea M, Kunze K, Heitmann U, Florek S, Franzke J, Niemax K (2005) J Phys D 38:1709–1715
53. Miclea M, Kunze K, Franzke J, Niemax K (2004) J Anal At Spectrom 19:990–994
54. Park S, Chen J, Wagner C, Ostrom N, Liu C, Eden J (2002) IEEE J Sel Top Quantum Electron 8:139–147
55. Eden J, Park S, Ostrom N, McCain S, Wagner C, Vojak B, Chen J, Liu C, von Allmen P, Zenhausern F, Sadler D, Jensen C, Wilcox D, Ewing J (2003) J Phys D 36:2869–2977
56. Longwitz R, Van Lintel H, Renaud P (2003) J Vac Sci Technol B 21:1570–1573
57. Wilson C, Gianchandani Y, Wendt A (2003) J Microelectromech Syst 12:835–839
58. Eijkel J, Stoeri H, Manz A (1999) Anal Chem 71:2600–2606
59. Eijkel J, Stoeri H, Manz A (2000) J Anal At Spectrom 15:297–300
60. Eijkel J, Stoeri H, Manz A (2000) Anal Chem 72:2547–2552
61. Bessoth F, Naji O, Eijkel J, Manz A (2002) J Anal At Spectrom 17:794–799
62. Naji O, Manz A (2004) Lab Chip 4:431–437
63. Mitra B, Gianchandani Y (2008) IEEE Sens J 8:1445–1454
64. Morris J, Krey R, Garrison R (1969) Phys Rev 180:167–183
65. Mitra B, Levey B, Gianchandani Y (2008) IEEE Trans Plasma Sci 36:1913–1924
66. Kushner M (2005) J Phys D 38:1633–1643
67. Abeysinghe D, Dasgupta S, Jackson H, Boyd J (2002) J Micromech Microeng 12:229–235
68. Fielder R, Stingson-Bagby K, Palmer M (2004) In: Proceedings of SPIE, fiber optic sensor technology and applications III, Philadelphia, pp 60–69
69. Li T, Wang Z, Wang Q, Wei X, Xu B, Hao W, Meng F, Dong S (2007) In: Proceedings of SPIE, sensors for harsh environments III, Boston, pp 1–7
70. Ned A, Okojie R, Kurtz A (1998) In: Proceedings of the international high temperature electronics conference, Albuquerque, pp 257–260
71. Fricke S, Friedberg A, Ziemann T, Rose E, Muller G, Telitschkin D, Ziegenhagen S, Seidel H, Schmidt U (2006) In: Proceedings of micro-nano-technology aerospace applications, Toulouse
72. Guo S, Eriksen H, Childress K, Fink A, Hoffman M (2008) Proceedings of the IEEE international conference on micro electro mechanical systems, Tucson, pp 892–895
73. Wright S, Gianchandani Y (2009) J Microelectromech Syst 18:736–743
74. Edelmann C (1990) Vacuum 41:2006–2008
75. Allen D (2003) Proc Inst Mech Eng B 217:643–650
76. Wright S, Gianchandani Y (2007) J Vac Sci Technol B 25:1711–1720
77. Yoon J, Lee D, Nam H, Cha G, Strong T, Brown R (1999) J Electroanal Chem 464:135–142

78. Taylor S, Srigengan B, Gibson J, Tindall D, Syms R, Tate T, Ahmad M (2000) In: Proceedings of SPIE, chemical and biological sensing, Orlando, pp 187–193
79. Miller R, Nazarov E, Eiceman G, King A (2001) Sens Actuators A. 91:301–312
80. Jenkins G, Manz A (2002) J Micromechanics Microengineering 12:N19–N22
81. Cserfalvi T, Mezei P (2003) J Anal At Spectrom 18:596–602
82. Kim H, Lee J, Kim M, Cserfalvi T, Mezei P (2000) Spectrochim Acta Part B 55:823–831
83. Johnson K, Wilp W, Karanassios V (2001) In: Proceedings of SPIE, Boston, pp 347–352
84. Karanassios V, Johnson K, Smith A (2007) Anal Bioanal Chem 388:1595–1604
85. Davis W, Marcus R (2001) J Anal At Spectrom 16:931–937
86. Marcus R, Davis W (2001) Anal Chem 73:2903–2910
87. Wilson C, Gianchandani Y (2002) IEEE Trans Electron Devices 49:2317–2322
88. Que L, Wilson C, Gianchandani Y (2005) J Microelectromech Syst 14:185–191
89. Zorn M, Wilson C, Gianchandani Y, Anderson M (2004) IEEE Sens Lett 2:179–185
90. Mitra B, Wilson C, Que L, Selvaganapathy P, Gianchandani Y (2006) Lab Chip 6:60–65
91. Haugland R (1996) Handbook of fluorescence probes and research chemicals. Molecular Probes, Eugene
92. Knoll G (2000) Radiation detection and measurement. Wiley, New York
93. Hirschfelder J, Magee J, Hull M (1948) Phys Rev 73:852–862
94. Shimoni U, Sheinfux B, Seidman A, Grinberg J, Avrahami Z (1974) Nucl Instrum Methods 117:599–603
95. Shafrir B, Seidman A (1975) Nucl Instrum Methods 129:177–186
96. Nakamura M (1983) J Appl Phys 54:3141–3149
97. Kiff S, He Z, Tepper G (2005) IEEE Trans Nucl Sci 52:2932–2939
98. van Vuure T, van Eijk C, Fraga F, Hollander R, Margato L (2001) IEEE Trans Nucl Sci 48:1092–1094
99. Veloso J, Amaro F, dos Santos J, Mir J, Derbyshire G, Stephenson R, Rhodes N, Schooneveld E (2004) IEEE Trans Nucl Sci 51:2104–2109
100. Charpak G, Bouclier R, Bressani T, Favier J, Zupancic C (1968) Nucl Instrum Methods 62:262–268
101. Oed A (1988) Nucl Instrum Methods Phys Res A 263:351–359
102. Francke T, Vladimir P (2003) In: Proceedings INFN ELOISATRON project workshop, Erice, pp 158–179
103. Charpak G, Derre J, Giomataris Y, Rebourgeard P (2002) Nucl Instrum Methods Phys Res A 478:26–36
104. Sarvestani A, Besch H, Junk M, MeiBner W, Pavel N, Sauer N, Stiehler R, Walenta A, Menk R (1998) Nucl Instrum Methods Phys Res A 419:444–451
105. Sauli F (2001) Nucl Instrum Meth Phys Res A 461:47–54
106. Breskin A (2000) Nucl Instrum Methods Phys Res A 454:26–39
107. Kyker R, Berry N, Stark D, Nachtigal N, Kershaw C (2004) Proceedings of SPIE, digital wireless communications VI, Orlando, pp 293–304
108. Nemzek R, Dreicer J, Torney D, Warnock T (2004) IEEE Trans Nucl Sci 51:1693–1700
109. Brittain J (2004) Proc IEEE 92:1501–1504
110. Heaton A, Reeves J (1974) In: International conference on gas discharges, London, pp 73–77
111. Eun C, Gianchandani Y (2008) J Micromechanics Microengineering 18:095007
112. Eun C, Gharpurey R, Gianchandani Y (2006) In: Proceedings of the IEEE international conference micro electro mechanical systems, Istanbul, pp 570–573
113. Eun C, Gharpurey R, Gianchandani Y (2006) In: Proceedings of solid-state sensors, actuators, microsystems workshop, Hilton Head, pp 236–239
114. Petersen K (1982) Proc IEEE 70:420–457
115. Belloy E, Sayah A, Gijs M (2000) Sens Actuators A 86:231–237
116. West J, Jadhav A (2007) J Micromechanics Microengineering 17:403–409
117. Zheng Z, Cheng W, Huang F, Yan B (2007) J Micromechanics Microengineering 17:960–966
118. Eun C, Gianchandani Y (2008) In: Proceedings of solid-state sensors, actuators, microsystems workshop, Hilton Head, pp 308–311
119. Richardson M, Gianchandani Y (2008) J Micromechanics Microengineering 18:015002